Quantum-classical distance as a tool to design optimal chiral quantum walks

Massimo Frigerio ⓘ,* Claudia Benedetti ⓘ,† Stefano Olivares ⓘ,‡ and Matteo G. A. Paris ⓘ§

Quantum Technology Lab & Applied Quantum Mechanics Group, Dipartimento di Fisica "Aldo Pontremoli,"
Università degli Studi di Milano, I-20133 Milano, Italy
and INFN, Sezione di Milano, I-20133 Milano, Italy

Continuous-time quantum walks (CTQWs) provide a valuable model for quantum transport, universal quantum computation, and quantum spatial search, among others. Recently, the empowering role of new degrees of freedom in the Hamiltonian generator of CTQWs, which are the complex phases along the loops of the underlying graph, was acknowledged for its interest in optimizing or suppressing transport on specific topologies. We argue that the quantum-classical distance, a figure of merit which was introduced to capture the difference in dynamics between a CTQW and its classical, stochastic counterpart, guides the optimization of parameters of the Hamiltonian to achieve better quantum transport on cycle graphs and spatial search for the quantum speed limit without an oracle on complete graphs, the latter also implying fast uniform mixing. We compare the variations of this quantity with the 1-norm of coherence and the inverse participation ratio, showing that the quantum-classical distance is linked to both, but in a topology-dependent relation, which is key to spot the most interesting quantum evolution in each case.

I. MOTIVATION AND LAYOUT

Continuous-time quantum walks (CTQWs) are intensively studied as simplified models for a wide range of applications, spacing from quantum transport [1–7], e.g., excitonic transport in biochemical complexes involved in some instances of bacterial photosynthesis [8–10], to universal quantum computation [11] or specific quantum algorithms such as the spatial search [12–18]. They are usually defined [19] on the same line of classical random walks (RWs) on undirected, simple graphs by promoting the graph Laplacian L, which is the generator of the time evolution of an unweighted RW, to a Hamiltonian H. Going from the classical transfer matrix to the quantum unitary evolution operator, together with the shift of focus from probabilities to amplitudes, make CTQW radically different from classical RW, with reliable prospects of achieving a quantum advantage in specific tasks [20]. To mention a few, it is known that CTQW exhibit ballistic propagation of probability on lattices, contrary to the diffusive behavior of classical RW, and that they can solve search problems in shorter times.

Fairly recently, however, it has been suggested that constraining the Hamiltonian of the CTQW to be the Laplacian of the graph is an unnecessary restriction, and richer phenomenology can be observed when the off-diagonal matrix elements of H are allowed to be generic complex phases, in compliance just with Hermiticity: the resulting systems are called *chiral* CTQWs [21,22], because they exhibit asymme-try under time-reversal and directional bias in the propagation of probability. Further motivation for this generalization of CTQW has been provided in Ref. [23], where the most general correspondence between classical and quantum continuous-time random walks was also derived. Acknowledging this larger space of opportunities offered by quantum walks, which stems from the one-to-many nature of the step from classical to quantum, one is immediately faced with a new challenge: if assuming $H = L$ leads to a single choice of CTQW for a given unweighted graph, enlarging the focus to include chiral CTQW offers many free, real parameters that can be adjusted to optimize the quantum advantage in a specific task, at fixed graph topology.

In this paper, we show through a variety of relevant examples and an analytic discussion that a previously introduced quantity [24], the quantum-classical distance $\mathcal{D}_{QC}$, is a valuable tool to guide this optimization: it correctly captures the distinction between classical and quantum evolutions of random walks on graphs. Quite generally, quantum walks outperform classical random walks because of faster hitting, which is related to quantum transport and targeting, and faster mixing [25,26], when the walker spreads out towards a maximally coherent, uniform superposition of all sites. By maximizing the value of $\mathcal{D}_{QC}$ at short timescales over the free parameter space, one is quickly directed towards chiral CTQWs which least resemble the corresponding classical RW and could therefore exhibit a quantum advantage, either because of quick hitting or mixing [25,26] depending on the graph's topology. Indeed, although from their very introduction in Ref. [19] the quantum advantage of CTQW has been linked with quantum coherence, it is clear that it cannot reduce to this sole quantum phenomenon, since the target state in a transport task on a graph has very little coherence, for example (although it *does* play a role throughout the evolution).

————————

*massimo.frigerio@unimi.it
†claudia.benedetti@unimi.it
‡stefano.olivares@fisica.unimi.it
§matteo.paris@fisica.unimi.it

After setting the notation for continuous-time classical and (chiral) quantum walks in Sec. II, we bring attention to the three dynamical quantities that will be employed throughout the article: the quantum-classical distance, the 1-norm of coherence, and the inverse participation ratio, which are all defined in Sec. III and accompanied by a comparison of their short-time expansions for generic chiral Hamiltonians. We then argue the effectiveness of $\mathcal{D}_{\mathrm{QC}}$ in the identification of "optimal" phase configurations at fixed topology by looking at four very different and emblematic examples. We start with cycle graphs in Sec. IV, which allow for analytical expressions also in the presence of phases and constitute a test bed for our ideas. For odd cycles we show that the quantum-classical distance correctly signals the best phase for quantum transport and, conversely, spots the characteristic suppression of transport in even cycles for a resonant phase value, which is associated with a dip in the value of $\mathcal{D}_{\mathrm{QC}}$.

Then in Sec. V we move to complete graphs, having maximal connectivity. After a preliminary exploration based on randomly generated Hamiltonians, we maximize the quantum-classical distance at short times and find a particular set of Hermitian Hamiltonians which permit quantum search without oracle in a time which exactly achieves the optimal quantum speed limit, outperforming Grover's algorithm in the constant prefactor and holding for any size of the complete graph. Interestingly, here $\mathcal{D}_{\mathrm{QC}}$ is larger for evolutions which quickly lead to highly *delocalized* states, in stark contrast with its behavior for cycles. This is consistent with the other typical behavior of quantum walks, which is *fast mixing*. Indeed, the same optimal chiral evolution on complete graphs achieves uniform mixing, contrary to the nonchiral evolution, also with a quadratic speedup with respect to the standard protocol that involves hypercube graphs [25].

As a third case, in Sec. VI we examine quantum switches, constructed from a triangle graph with independent chains of sites attached to each vertex of the polygon. It is already known that, for resonant value of the sole free phase, this topology allows for directional quantum transport from one arm of the triangle to another, with minimal losses on the excluded, third arm. We show that the quantum-classical distance again spots the best value of the phase. Moreover, since these graphs are nonregular, an ambiguity about the diagonal entries of H arises, since the nonchiral association $H = L$ indirectly introduces a potential field landscape. We argue that setting all the diagonal phases of H to the same, arbitrary value, instead of the nonuniform connectivities of the different sites, is the unbiased choice and also the most efficient one for directional quantum transport.

Finally, we tackle the cube graph in Sec. VII, on which perfect quantum transport from one vertex to the opposite one, with the Laplacian as generator, is known to happen. The quantum-classical distance here suggests that phases cannot improve this standard evolution. However, minimal values of $\mathcal{D}_{\mathrm{QC}}$ are achieved in correspondence with evolutions that suppress transport at all times on half of the vertices of the cube.

It is worth stressing that we are not stating that chiral CTQWs achieving higher values of $\mathcal{D}_{\mathrm{QC}}(t)$ will necessarily provide a quantum advantage. Rather, *considering the little guidance that we currently have in devising new quantum algo-*

rithms and the enormous parameter space of chiral CTQWs on large graphs, we claim that the quantum-classical distance can offer a simple criterion to spot the quantum evolution which is the least similar to the classical one and therefore could potentially display a quantum advantage.

II. QUANTUM AND CLASSICAL WALKS ON GRAPHS

Continuous-time quantum walks are traditionally introduced through an analogy with classical random walks on graphs. For the latter, one considers an undirected simple graph $\mathcal{G} = (V, E)$ of N vertices, where V is the set of vertices or *sites*, and E is the set of edges. To $\mathcal{G}$ corresponds an $N \times N$ symmetric matrix, namely the *Laplacian matrix* of the graph, which is defined as $L = D - A$ where A is the adjacency matrix of $\mathcal{G}$, such that $[A]_{jk} = 1$ if there is an edge in E connecting sites j and k and 0 otherwise, including the diagonal elements, whereas D is a diagonal matrix encoding the connectivities of each vertex, i.e., the number of edges departing from it. Since the sum of the rows and of the columns of L is zero, it generates a semigroup of bistochastic transformations $\mathcal{E}_t = e^{-tL}$ for $t \in \mathbb{R}^+$. Therefore, acting on a vector $\underline{p}_0 \in \mathbb{R}^N$ of occupation probabilities for each site at the initial time, one has a continuous-time autonomous stochastic process on the graph, which we will call a continuous-time (classical) random walk:

$$\underline{p}(t) := \mathcal{E}_t[\underline{p}] := e^{-tL} \underline{p}_0. \qquad (1)$$

Farhi and Gutmann [19] noticed a suggestive similarity between Eq. (1) and the Schrödinger equation for an N-level quantum system. Therefore, they proposed to *define* a continuous-time quantum walk on the same graph $\mathcal{G}$ by promoting L to a quantum Hamiltonian matrix $H = L$ acting on an N-dimensional complex Hilbert space $\mathcal{H} \sim \mathbb{C}^N$ which has a preferred basis $\{|j\rangle\}_{j=1,\dots,N}$ whose elements describe localized quantum states on the sites of the graph. The quantum evolution of any initial state $|\psi_0\rangle \in \mathcal{H}$ now comes automatically:[1]

$$|\psi(t)\rangle = U_t |\psi_0\rangle = e^{-it\hat{H}} |\psi_0\rangle. \qquad (2)$$

Recently it was pointed out that imposing $H = L$ is too restrictive on the quantum side, since a generic Hamiltonian compatible with the graph topology does not need to be a real matrix, but just a Hermitian one. We will focus on *unweighted* graphs, such that the nonzero elements of the adjacency matrix A are equal to 1 for all the links. Therefore, the most general H has off-diagonal entries:

$$[H]_{kj} = e^{i\varphi_{kj}} \quad (j \neq k), \qquad (3)$$

if sites j and k are linked in $\mathcal{G}$, and zero otherwise. Here $\varphi_{kj} \in [0, 2\pi)$ is a phase depending on the link and $\varphi_{kj} = -\varphi_{jk}$ is required by Hermiticity of H. On the other hand, the diagonal elements of H must be real numbers, but they do not need to satisfy any further constraint. For regular graphs, the

---

[1]Here and in the following we fix $\hbar = 1$. The units of energies are reabsorbed in the timescale so as to conveniently keep everything dimensionless.

simplest and most unbiased choice is to assume $[H]_{jj} = d$ for all $j = 1, \ldots, N$ so that they are all equal and they can be discarded as they generate an overall, unobservable phase shift on the whole Hilbert space. For nonregular graphs, instead, the choice is less obvious and we shall return to this point in a later section (see also Ref. [27]). Continuous-time quantum walks whose Hamiltonian is a generic Hermitian matrix compatible with the graph topology are also called *chiral* CTQWs to distinguish them from the most standard case with $H = L$ (or $H = A$), which is by far the most studied in the literature as of now.

In this work, we are interested in optimizing the additional degrees of freedom of a chiral CTQW on a given graph to achieve the maximal advantage over the corresponding, unique classical RW. It is thus convenient to formulate both evolutions in the Hilbert space formalism to facilitate the comparison. To do this, we first remark that quantum coherent states in the site basis do not exist at the classical level, therefore we shall assume a localized state $|j\rangle$ with $j = 1, \ldots, N$ as the initial condition for both the quantum and the classical evolution, to make a fair comparison. Then the classical evolution can be defined by the standard embedding of a classical probability onto a Hilbert space with respect to a preferred basis, that is

$$\mathcal{E}_t[|j\rangle\langle j|] = \sum_{k=1}^{N} \langle k|e^{-tL}|j\rangle|k\rangle\langle k| = \sum_{k=1}^{N} p_{kj}(t)|k\rangle\langle k|, \quad (4)$$

which ensures that the classically evolved state is always incoherent in the localized basis. Also the quantum evolution can be rewritten in a similar way:

$$\mathcal{U}_t[|j\rangle\langle j|] = e^{-i\hat{H}t}|j\rangle\langle j|e^{i\hat{H}t} = |\psi_j(t)\rangle\langle\psi_j(t)|, \quad (5)$$

where

$$|\psi_j(t)\rangle = \sum_{k=1}^{N} \alpha_{kj}(t)|k\rangle, \quad (6)$$

$$\alpha_{kj}(t) = \langle k|e^{-i\hat{H}t}|j\rangle = \left[e^{-iHt}\right]_{kj}. \quad (7)$$

Chiral quantum walks and gauge invariance of transition probabilities

By a diagonal, unitary change of basis, which is a local phase transformation, many of the phases of H can be set to 0. This is particularly useful when considering site-to-site transition probabilities, as it is often the case when dealing with quantum walks. Indeed, quantities such as $P_{j \to k}(t) = |\langle k|e^{-iHt}|j\rangle|^2$ and functions thereof do not depend on phases which can be removed by those local phase transformations. These are effectively *gauge transformations* and, at least for some regular topologies of the underlying graphs, the change in the Hamiltonian's phases can be accounted for by a gauge transformation of the *gauge connection field*. Since to each edge of the graph can correspond a phase in H and the phase of the localized state on each vertex can be modified independently, the maximal number of phase degrees of freedom that affect the transition probabilities $P_{j \to k}(t)$ is $|E| - N + 1 = 1 - \chi(\mathcal{G})$, where $|E|$ is the number of edges of the graph, whereas $\chi(\mathcal{G})$ is the Euler characteristic for generic graphs, including nonplanar ones. For planar graphs, this number is

precisely the number of loops, while for nonplanar ones the number of loops is not obvious to define. In particular, phases cannot affect transition probabilities on tree graphs, while cycle graphs all have just a single relevant phase, which can be distributed over each link or concentrated on a single one. However, given a particular choice for the Hermitian matrix H, it is not trivial to determine whether it is equivalent to a real, symmetric Hamiltonian. It has been shown [28] that this is the case if and only if the product of phase factors along each directed, simple, closed path on $\mathcal{G}$ is 1.

III. QUANTUM-CLASSICAL DISTANCE

By combining Eq. (4) and Eqs. (5) and (6), it is possible to define a time-dependent quantity which compares the quantum evolution to the classical one, when both start in the same, localized initial state $\hat{\rho}_j^0 = |j\rangle\langle j|$. This quantity is the *quantum-classical distance* [24]:

$$\mathcal{D}_{\text{QC}}^j(t) := 1 - \mathcal{F}\left[\mathcal{E}_t(\hat{\rho}_j^0), \mathcal{U}_t(\hat{\rho}_j^0)\right] \quad (8)$$

$$= 1 - \sum_{k=1}^{N} p_{kj}(t)|\langle k|\psi_j(t)\rangle|^2. \quad (9)$$

It is related to the fidelity $\mathcal{F}[\hat{\rho}, \hat{\sigma}] = \text{Tr}[(\sqrt{\hat{\rho}}\hat{\sigma}\sqrt{\hat{\rho}})^{1/2}]^2$ between the classical and the quantum evolved states [24]. Equation (9) follows from Eq. (8) when the initial state is localized, but it is clearly not valid when the initial state is mixed, in which case Eq. (8) should be used directly. Notice that $\mathcal{D}_{\text{QC}}^j(t)$ is zero at a given time if and only if the classically and quantum evolved states are exactly the same at that time. Despite the fact that, analogously to other measures of similarity between two probability distributions, its value becomes uninformative whenever one of the two states is proportional to the identity, being equal to $1 - \frac{1}{N}$ in this instance,[2] this quantity should be considered throughout its whole time evolution, showing the departure between the quantum and the classical dynamics. It is still true, by the same token as in Ref. [24], that the maximum value of the quantum-classical distances over all possible *classical* initial states can be attained by a single localized state, at any given time. Therefore we can still define a global quantum-classical distance by[3]

$$\mathcal{D}_{\text{QC}}(t) := \max_{j \in V} \left\{\mathcal{D}_{\text{QC}}^j(t)\right\}, \quad (10)$$

which is independent of the initial state but only depends on the graph (specified by L) and the choice of H compatible with the topology. Among pure initial states, instead, the maximum has to be restricted over localized ones, since the classical evolution cannot be defined on superpositions, while considering mixed initial states that are diagonal in the site basis will be less informative about the details of the two evolutions.

---

[2]This is true also for the relative entropy of the (pure) quantum evolved state with respect to the classical one, which can be used as an alternative measure of the distance between the two dynamics, leading to essentially identical conclusions. Here N is the size of the graph.

[3]V is the ordered set of vertices of the graph.

Checking for a few graphs with different topologies and number of vertices, the overall behavior of this quantity in time seems very similar to the simpler scenario where L is a Laplacian and the straightforward identification $H = L$ can be applied. In particular, the asymptotic value in the long-time limit takes the same expression for any connected graph of size N and it is given by

$$\mathcal{D}_{\mathrm{QC}}^j(t \gg 1) \simeq 1 - 1/N. \tag{11}$$

Because of this saturation effect of $\mathcal{D}_{\mathrm{QC}}$ at large times, fluctuations of the quantum-classical distance can be significant only if they happen before the classical evolution gets close to equilibrium. This is a valuable property: indeed, since the quantum evolution is aperiodic on general graphs, unpredictable behavior can occur at sufficiently long times and it is therefore mandatory, from a physical point of view, to impose a cutoff on the relevant timescale to perform the required task. A natural choice is precisely the timescale of the classical evolution, especially if a quantum advantage is sought.

A. Quantum-classical distance at short times

To understand the behavior of the quantum-classical distance at short times, instead, we may expand $p_{kj}(t)$ and $|\langle k|\psi_j(t)\rangle|^2$ up to second order in t and obtain

$$\mathcal{D}_{\mathrm{QC}}^j(t) = t([H^2]_{jj} - [H]_{jj}^2) - t^2\left(-[H^2]_{jj} + [H]_{jj}^2\right.$$
$$\left. + \frac{1}{2}[H^2]_{jj}^2 - [H^2]_{jj}[H]_{jj}^2 + \frac{1}{2}\sum_s |H_{js}|^4\right) + O(t^3). \tag{12}$$

If we focus on unweighted graphs, which means that we assume $|H_{jk}|$ to be either 1 or 0 depending on whether vertices j and k are connected by an edge or not, then we can considerably simplify the expression above. Indeed, we find that

$$[H^2]_{jj} - [H]_{jj}^2 = d_j = L_{jj}, \tag{13}$$

where d_j is the connectivity of vertex j in the graph. Notice also that

$$\frac{1}{2}[H^2]_{jj}^2 - [H^2]_{jj}[H]_{jj}^2 + \frac{1}{2}\sum_s |H_{js}|^4 \tag{14}$$

$$= \frac{1}{2}\left([H^2]_{jj} - [H]_{jj}^2\right)^2 + \frac{1}{2}\sum_{s \neq j} |H_{js}|^4 \tag{15}$$

$$= \frac{d_j^2 + d_j}{2}, \tag{16}$$

where, in the last step, we used the fact that $\sum_{s \neq j} |H_{js}|^4$ gets a contribution of 1 for any s connected to j and 0 otherwise. Therefore, the short-time expansion of the quantum-classical distance to second order is

$$\mathcal{D}_{\mathrm{QC}}^j(t) = d_j t - d_j(d_j - 1)\frac{t^2}{2} + O(t^3). \tag{17}$$

It is relevant to stress that the coefficients of this expansion are dictated just by the connectivity of the starting vertex and they are not influenced by any other parameter involved in H: in

particular, *neither the on-site average energies nor the phases of the off-diagonal entries of H affect the short-time behavior of the quantum-classical distance*; however, the timescale at which the second-order expansion can be trusted is typically orders of magnitude smaller than the timescale at which we maximize its value in the following examples.

B. 1-norm of coherence and inverse participation ratio

To understand what type of properties of the quantum walk contribute to the quantum-classical distance and how $\mathcal{D}_{\mathrm{QC}}$ relates to some figures of merit that are considered useful for particular tasks, we now seek the short-time expansion of other two quantities, the 1-norm of coherence and the inverse participation ratio (IPR), to be later compared with Eq. (17).

Let us start with the 1-norm of coherence. With respect to the localized basis, the coherence of the pure state $|\psi_j(t)\rangle$ given by Eq. (5) can be written as [24]

$$\mathcal{C}_j(t) = \left(\sum_k |\alpha_{kj}(t)|\right)^2 - 1, \tag{18}$$

with $\alpha_{jk}(t)$ defined according to Eq. (6). Here and in the following, it will be helpful to start from the fourth-order short time expansion of $|\alpha_{kj}(t)|^2$:

$$|\alpha_{kj}(t)|^2 = \delta_{jk} - t^2\left(\delta_{jk}[H^2]_{jj} - |H_{jk}|^2\right)$$
$$+ t^3\mathrm{Im}\left[H_{jk}[H^2]_{kj}\right]$$
$$+ t^4\left(\frac{1}{12}\delta_{jk}[H^4]_{jj} - \frac{1}{3}\mathrm{Re}\left[H_{jk}[H^3]_{kj}\right]\right.$$
$$\left. + \frac{1}{4}\left|[H^2]_{jk}\right|^2\right) + O(t^5). \tag{19}$$

From this, it follows that

$$\sum_k |\alpha_{kj}(t)| = \sqrt{1 - d_j t^2 + O(t^4)}$$
$$+ t\sum_{k \neq j} |H_{jk}|\sqrt{1 - t\,\mathrm{Im}\left[H_{jk}[H^2]_{kj}\right] + O(t^2)}$$
$$+ \frac{t^2}{2}\sum_{k \neq j, H_{jk}=0} \left|[H^2]_{jk}\right| + O(t^3), \tag{20}$$

where we split the initial sum over k in a first term with $k = j$, a second sum with $k \neq j$ but which gets contributions only for terms having $H_{jk} \neq 0$, and a final sum that takes into account the last terms with $k \neq j$ and $H_{jk} = 0$. Expanding the square roots and collecting powers of t, one obtains

$$\sum_k |\alpha_{kj}(t)| = 1 + t d_j - \frac{1}{2}t^2\left(d_j + \sum_{k \neq j} \mathrm{Im}\left[H_{jk}[H^2]_{kj}\right]\right.$$
$$\left. + \sum_{\substack{k \neq j \\ H_{jk}=0}} \left|[H^2]_{jk}\right|\right) + O(t^3). \tag{21}$$

Now notice that

$$
\sum_{k \neq j} \mathrm{Im}\big[H_{jk}[H^2]_{kj}\big] = \sum_{k} \mathrm{Im}\big[H_{jk}[H^2]_{kj}\big]
$$
$$
= \mathrm{Im}\big[H^3\big]_{jj} = 0.
$$

Overall, for coherence we find

$$
\mathcal{C}_j(t) = 2 d_j t
$$
$$
+ \left[d_j(d_j - 1) - \sum_{\substack{k \neq j \\ H_{jk}=0}} \big|[H^2]_{jk}\big| \right] t^2 + O(t^3). \quad (22)
$$

One can appreciate the fact that coherence has a very similar structure to quantum-classical distance at short times, but it is affected by other degrees of freedom of H. Indeed, the term $\sum_{\substack{k \neq j \\ H_{jk}=0}} |[H^2]_{jk}|$ has a simple graphical interpretation: $|[H^2]_{jk}|$ for $k \neq j$ and for $H_{jk} = 0$ it is a sum over all possible paths of length 2 connecting vertex j with a vertex k at distance 2 from j, where each path is weighted by the product of the phases of its two links in the direction from j to k. Since this is the modulus of a sum of phases, interference may happen. Therefore $\mathcal{C}_j$ can get a phase-dependent second-order contribution in t only if the graph contains a four-cycle passing through j and bearing a nonzero overall phase, so that there will be at least two paths joining the same k with j and weighted by different phase factors.

To quantify the spreading in time of the QW from the initial vertex, a useful figure of merit is provided by the inverse participation ratio:

$$
\mathcal{I}_j(t) = \sum_k |\alpha_{kj}(t)|^4, \quad (23)
$$

which decreases while the QW spreads over the vertices of the graph. The second-order short-time expansion of $\mathcal{I}_j(t)$ is derived from Eq. (19):

$$
\mathcal{I}_j(t) = 1 - 2 d_j t^2 + O(t^4). \quad (24)
$$

The above expression is clearly related to coherence and $\mathrm{D}_{\mathrm{QC}}^j$, but, unlike for coherence, the IPR is determined just by the connectivity of the starting vertex at least up to second order in t.

The conclusion we can draw is that the short-time expansion of the quantum-classical distance correlates with coherence and IPR, but in a way that depends nontrivially upon the topology; indeed $\mathcal{D}_{\mathrm{QC}}(t)$, for a localized initial condition, depends on the classical and quantum *probability distributions* at a given time, and these can be similar irrespective of the coherences. In the following, we argue that this is in fact a merit of $\mathcal{D}_{\mathrm{QC}}$.

IV. CYCLE GRAPHS

The simplest example to investigate the role of phases in the Hamiltonian of CTQW for quantum transport is provided by cycle graphs. As discussed previously, by gauge invariance we can write the generic Hamiltonian H for a chiral CTQW

on a cycle graph as follows:

$$
H = \begin{pmatrix}
d_1 & e^{i\theta} & 0 & 0 & \dots & e^{-i\theta} \\
e^{-i\theta} & d_2 & e^{i\theta} & 0 & \dots & 0 \\
0 & e^{-i\theta} & d_3 & e^{i\theta} & \dots & 0 \\
\vdots & \vdots & & & \vdots & \vdots \\
e^{i\theta} & 0 & 0 & \dots & e^{-i\theta} & d_N
\end{pmatrix}, \quad (25)
$$

where $\theta \in [0, 2\pi)$ is the only relevant phase, which has been distributed equally over all links for convenience, while $d_1, \dots, d_N \in \mathbb{R}^+$. In this work we focus on the role of phases, hence we will take $d_1 = \cdots = d_N = d$ and further impose $d = 0$ without loss of generality. The eigenvectors of H will still be Bloch states:

$$
|\lambda_j\rangle := \frac{1}{\sqrt{N}} \sum_{k=1}^{N} e^{i \frac{2\pi jk}{N}} |k\rangle, \quad (26)
$$

while the eigenvalues will be shifted according to

$$
\lambda_j := 2 \cos\left(\theta + \frac{2\pi j}{N} \right), \quad (27)
$$

where $j = 1, \dots, N$. Notice that, although for $\theta = 0$ the spectrum is doubly degenerate, for almost every $\theta \neq 0$ the degeneracy is lifted. Moreover, despite $\theta \in [0, 2\pi)$, one can always choose a representative phase in the reduced scheme, that is, $\theta \in [0, \frac{2\pi}{N})$, much like the first Brillouin zone for crystal momentum, without affecting transition probabilities between sites (see below). When N is large, the effect of θ on the spectrum is clearly minor. The transition probabilities associated with this chiral quantum walk on a cycle are

$$
P_{j \to k}(t) := \frac{1}{N^2} \left| \sum_{s=1}^{N} e^{2i\left\{ \frac{\pi(k-j)s}{N} - t \cos\left(\theta + \frac{2\pi s}{N} \right) \right\}} \right|^2. \quad (28)
$$

We again stress the fact that, by virtue of gauge invariance, all the quantities that can be computed from these probabilities, assuming a localized initial state as before, would be the same for a more general H on the ring of the form:

$$
H = \begin{pmatrix}
d & e^{i\phi_1} & 0 & 0 & \dots & e^{-i\phi_N} \\
e^{-i\phi_1} & d & e^{i\phi_2} & 0 & \dots & 0 \\
0 & e^{-i\phi_2} & d & e^{i\phi_3} & \dots & 0 \\
\vdots & \vdots & & & \vdots & \vdots \\
e^{i\phi_N} & 0 & 0 & \dots & e^{-i\phi_{N-1}} & d
\end{pmatrix},
$$

by simply putting $\theta = \frac{1}{N} \sum_{j=1}^{N} \phi_j$ in Eq. (28).

In the large-ring limit, $N \to \infty$, since the single relevant phase θ can be concentrated as $N\theta$ on any single link at will by leveraging gauge invariance, the transition probabilities will be the same as for the standard continuous-time quantum walk on a ring:

$$
\lim_{N \to \infty} P_{j \to k}(t) = |J_{|k-j|}(2t)|^2, \quad (29)
$$

where $J_n(x)$ is the nth Bessel function. The same result can also be derived directly from Eq. (28). This also implies that the effect of phases on the quantum evolution starting on any fixed vertex will show up only when the probability will have reached the opposite side of the cycle, so that phase-dependent interference can happen. Since the initial propagation on the cycle is known to be ballistic with velocity 2, in order to
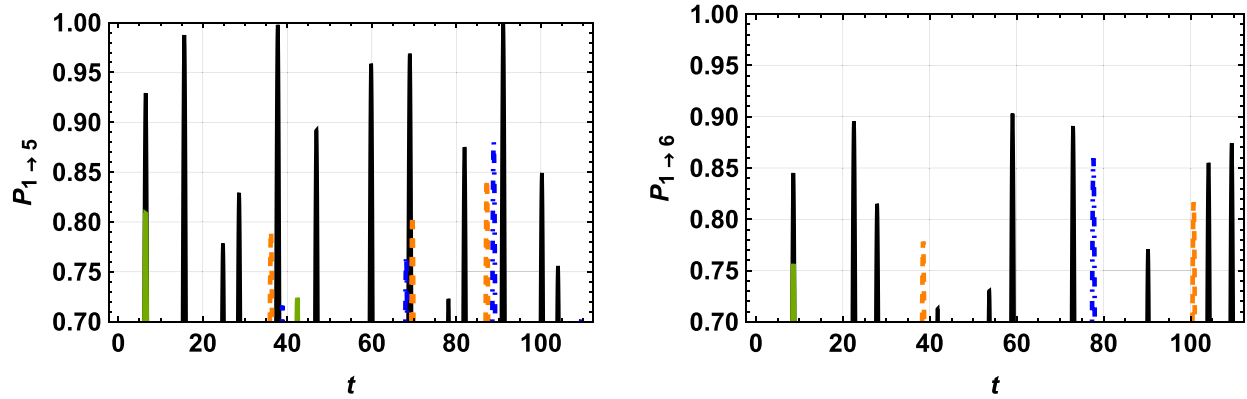
FIG. 1. Transition probability from initial site 1 to site 5 of an 8-cycle (left) and to site 6 of a 10-cycle (right) as functions of time and for different values of the phases. The nonchiral $\theta = 0$ case is plotted in black. For the 8-cycle the other phases are $\theta = 0.04$ (solid light green), $\theta = 0.13$ (dashed orange), and $\theta = 0.23$ (dotted-dashed blue). For the 10-cycle we chose $\theta = 0.027$ (solid, light green), $\theta = 0.13$ (dashed, orange) and $\theta = 0.28$ (dot-dashed, blue). Notice that the probability axis plot range is restricted to [0.7,1] because it is the most informative region for quantum transport.

reach the opposite side of the cycle the walker will take a time approximately given by $\tau = N/4$, which therefore is also the time it takes for $\theta \neq 0$ to have some appreciable effect on the on-site probabilities. However, this prediction can be inaccurate for small rings, because of the non-negligible tails of the ballistic wavefronts.

To understand the influence of phases on quantum transport on the cycle after this minimal time, let us first consider the standard $\theta = 0$ case. Here, starting with an initially localized state $|j\rangle$, all sites that are symmetrical with respect to the initial vertex must have the same occupation probability at all times, since the symmetry is preserved by the nonchiral Hamiltonian. In particular, the probability of finding the walker on each site except the starting one (and the one opposite to it in the case of even cycles) cannot exceed $\frac{1}{2}$ at any time. When the phase is added and N is even, for any θ one can show that this symmetry is preserved. Indeed, even cycles belong to the family of bipartite graphs, defined as those graphs whose vertices can be divided into two sets such that two vertices in the same set are never connected by an edge. For such graphs, one can apply a gauge transformation that flips the sign of all the basis elements of one set, while leaving the other set untouched, thereby implementing the transformation $H \rightarrow -H$, equivalent to time reversal, without affecting the transition probabilities. In particular, for even cycles, this implies that the probability of landing at site k or at its symmetric counterpart $N - k + 1$ is the same at all times also for $\theta \neq 0$. Therefore, any chiral quantum walk on an even cycle with N sites starting at site j can never be localized with probability greater than $\frac{1}{2}$ on any site different from the initial one and its opposite at $k = j + \frac{N}{2}$. As for the opposite site, which can be interesting as a target for transport, the situation is less clear. At fixed time, the optimal phase to maximize the probability $P_{j \rightarrow j+N/2}(t)$ can be different from zero. However, it seems that the highest peaks of $P_{j \rightarrow j+N/2}(t)$ for a wide range of times are always attained for $\theta = 0$. This can be appreciated in Fig. 1, where we plotted the transition probabilities between opposite sites vs time for cycles of 8 and 10 sites and for different values of θ. We restricted the plotting

region to probability values in [0.7,1] because we considered 0.7 as a lower bound to the acceptable fidelity of transport. Again, transition probabilities between other pairs of sites are neglected because they are always upper-bounded by $\frac{1}{2}$.

These observations suggest that chiral CTQWs provide no advantage for optimal quantum transport on even cycles over their nonchiral counterparts. Nevertheless, we highlight the fact that $P_{j \rightarrow j+N/2}(t)$ can be completely suppressed at all times by choosing $\theta = \pi/N$ (or, equivalently, a phase of π on a single, generic link), a phenomenon that, together with the unbroken reflection symmetry for generic θ, has already been attributed to the fact that even cycles are *bipartite* graphs. We notice that, in the context of excitonic transport in biochemical complexes, this sets a possible prediction to be contrasted with observations, since finding a ring-like structure with an even number of units could exclude that phases play a role.

When the cycle is odd, the conclusion can change dramatically. Here there is no opposite vertex to the starting one and, by the previous argument, the nonchiral QW ($\theta = 0$) can never localize on a site different from the initial one with probability greater than $\frac{1}{2}$. However, almost every $\theta \neq 0$ breaks the reflection symmetry with respect to the starting point, opening the possibility for enhanced quantum site-to-site transport. In Fig. 2 we plotted the transition probabilities from site 1 to various other sites of a 5-cycle and a 7-cycle for values of $\theta = \frac{\pi}{10}, \frac{\pi}{14}$, respectively [Figs. 2(a) and 2(b)]. For any other value of the phase in the relevant range $[0, \frac{2\pi}{N}]$, in each case the highest peaks are considerably lowered. It seems that the value $\frac{\pi}{2N}$ (where $N = 5, 7$ respectively) is *resonant*, although the pattern is very disordered and small changes in the precise value of the phase induce considerable shifts in the peaks at long times, which is a signature of chaos. This is illustrated by Figs. 2(c) and 2(d), where we displayed the same set of transition probabilities for the same cycles, but with a slightly off-resonant value of θ ($\theta = 0.29$ for the 5-cycle to be compared with the resonant value of $\frac{\pi}{10} \simeq 0.31$ and $\theta = 0.21$ for the 7-cycle to be compared with the resonant value of $\frac{\pi}{14} \simeq 0.22$). We stress that all these peaks displayed in the plots for odd cycles are entirely due to the introduction of
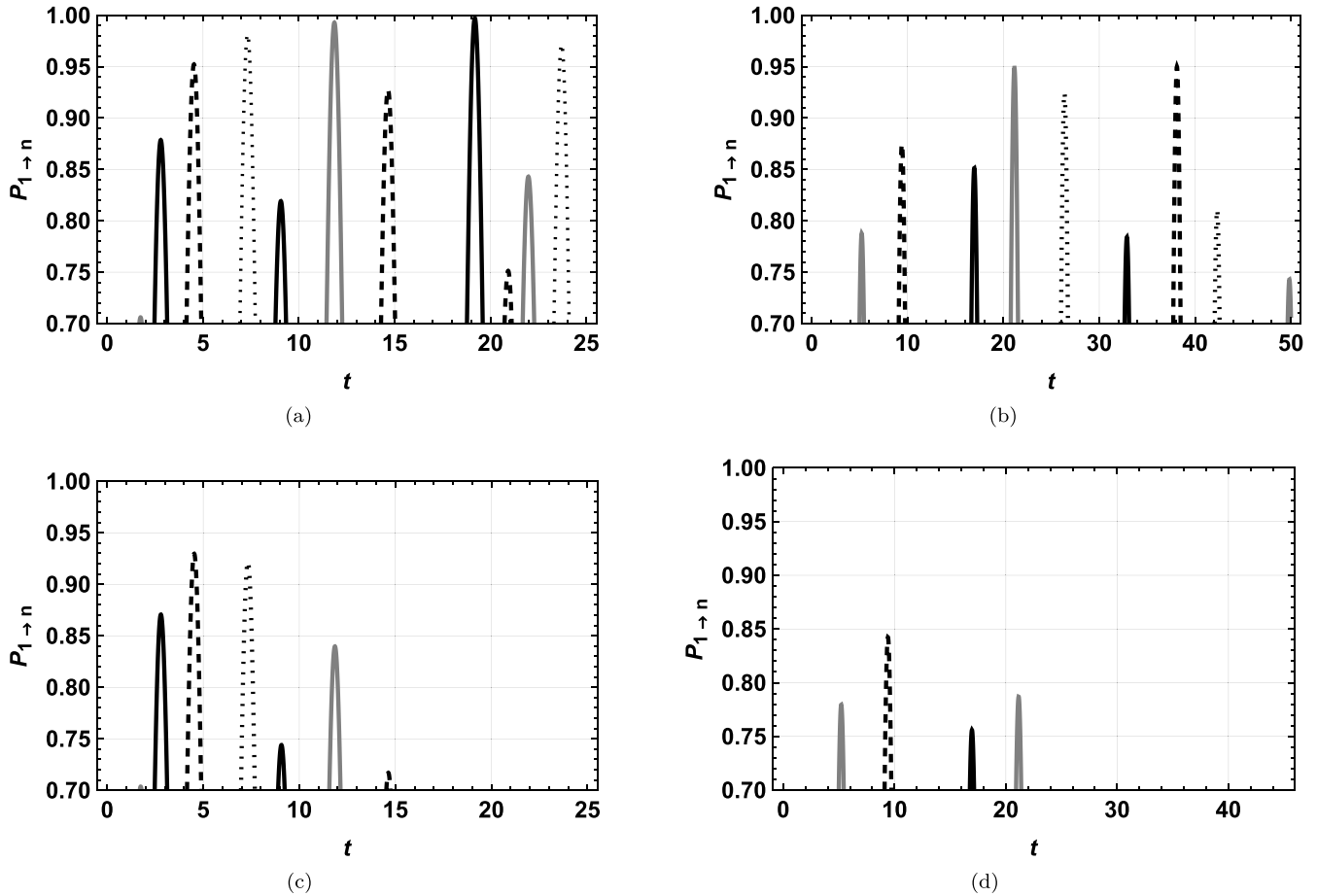
FIG. 2. Transition probability from initial site 1 to site n on a (a), (c) 5-cycle and on a (b), (d) 7-cycle as functions of time, for the resonant phase values [$\frac{\pi}{10}$ for the (a) 5-cycle and $\frac{\pi}{14}$ for the (b) 7-cycle) and for slightly off-resonant phase values (0.29 for the (c) 5-cycle and 0.21 for the (d) 7-cycle). Different stroke styles represent different target sites: $n = 2$ in solid black, $n = 3$ in gray, $n = 4$ in dashed black, and $n = 5$ in dotted black.

the phase degree of freedom, since *nonchiral* CTQWs on odd cycles starting in a localized state will never be found with probability higher than $\frac{1}{2}$ on other sites.

We will now see how the quantum-classical distance can capture these results for the prototypical example of cycle graphs and how it can indicate the optimal phase, putting order to the opaque relationship between the values of θ and the transition probabilities. A reasonably compact expression for the quantum-classical distance at time t as a function of θ can be derived from Eq. (28) and the standard formulas for a continuous-time classical random walk on cycles:

$$\mathcal{D}_{\text{QC}}(t;\theta) := 1 - \frac{e^{-2t}}{N^2} \sum_{k,s=1}^{N} \exp\left[2t \cos\frac{2\pi k}{N} \right.$$
$$\left. - 4it \sin\left(\theta + \frac{\pi(2s+k)}{N}\right) \sin\frac{\pi k}{N}\right]. \quad (30)$$

Since the dynamics is the same independently of the starting vertex, the expression for the quantum-classical distance can be computed for any localized initial state $|j\rangle$ and maximization over j is not necessary. It is a simple task to show

that

$$\mathcal{D}_{QC}\left(t; \frac{\pi}{N} + \phi\right) = \mathcal{D}_{\text{QC}}\left(t; \frac{\pi}{N} - \phi\right),$$

and, when N is odd, also

$$\mathcal{D}_{\text{QC}}\left(t; \frac{\pi}{2N} + \phi\right) = \mathcal{D}_{\text{QC}}\left(t; \frac{\pi}{2N} - \phi\right).$$

Therefore, when N is even, $\mathcal{D}_{\text{QC}}(t;\theta)$ attains all its possible values at fixed t and for θ in the range $[0, \frac{\pi}{N}]$, and when N is odd for θ in the range $[0, \frac{\pi}{2N}]$. Already for modestly sized polygons ($N \geqslant 7$), the variations of $\mathcal{D}_{\text{QC}}(t)$ with θ are very small. Indeed one can expand $\mathcal{D}_{\text{QC}}(t)$ around $t = 0$ and notice that all terms up to order $N - 1$ in t when N is even, and up to order $2N - 1$ in t when N is odd, are independent of θ, while an oscillatory θ dependence starts at higher orders. Because of this feeble θ dependence, we consider the difference between the quantum-classical distance with phase θ and the same quantity with zero phase, i.e., $\Delta\mathcal{D}_{QC}(t;\theta) = \mathcal{D}_{QC}(t;\theta) - \mathcal{D}_{QC}(t;0)$. As can be appreciated in Fig. 3, this quantity brings a clear order to the irregular behavior that was seen in the transition probabilities.

This ordering is also insightful when one considers the following: for even cycles, $\mathcal{D}_{QC}(t;\theta) - \mathcal{D}_{QC}(t;0)$ has a negative, significant dip at approximately the same time for all values
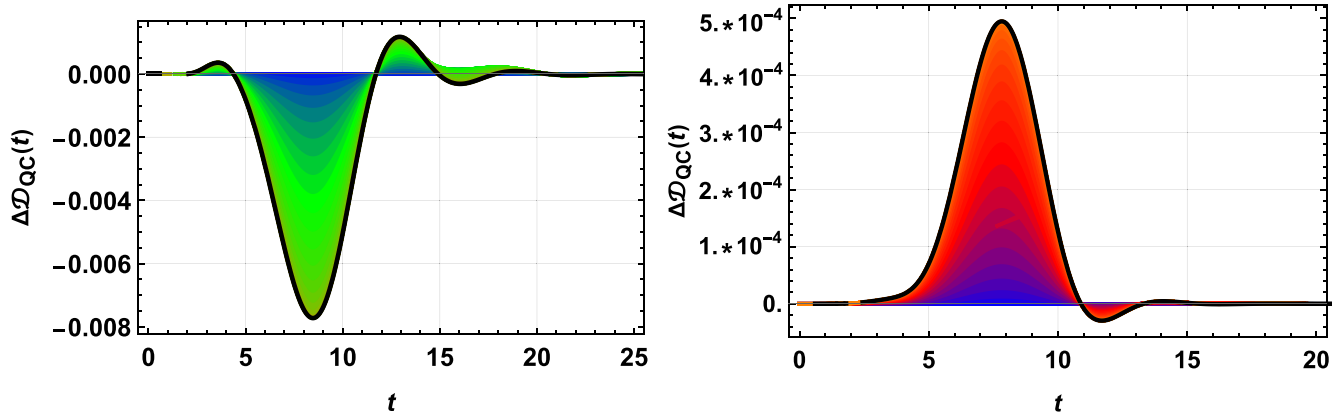
FIG. 3. Gain in quantum-classical distance $\Delta \mathcal{D}_{QC}(t)$ vs time for a 10-cycle (left) and a 7-cycle (right) with respect to the quantum-classical distance for the standard evolutions generated by the Laplacian (blue, horizontal baseline in both plots). For the 10-cycle, phases are increasing in the relevant range $[0, \frac{\pi}{10}]$ with a corresponding color hue from blue to green (from darker to lighter shade). For the 7-cycle, the relevant range of phases is $[0, \frac{\pi}{14}]$ and θ increases from blue to red hues (from darker to lighter shade). Notice that the maximum in time of $\mathcal{D}_{QC}$ is not necessarily related with the time at which transport occurs because the former quantity is also influenced by the timescale of the classical evolution.

of θ, and it is the lowest at $\theta = \frac{\pi}{N}$, the phase which fully suppresses transport to the opposite vertex; conversely, for odd cycles we find that the same quantity *peaks* at approximately the same time, with the highest peak for $\theta = \frac{\pi}{2N}$, again the resonant phase, which optimizes transport for odd cycles. Moreover, the heights of the peaks are monotonically increasing in absolute value with $\theta \in [0, \frac{\pi}{2N})$, while the depths of the dips for even N are monotonically increasing with $\theta \in [0, \frac{\pi}{N})$. Therefore, we see that finding the global maximum of $\Delta \mathcal{D}_{QC}$, with respect to θ and t, at a maximum (minimum) of $\mathcal{D}_{QC}(t; \theta)$ in time, correctly spots the least classical (the nearest to classical) evolution among all possible chiral CTQW on the same cycle. Intuitively, we can understand the reason for its effectiveness: $\mathcal{D}_{QC}(t)$ is maximized for the quantum evolution that departs the most from the classical one, the latter being slowly and diffusively spreading towards the homogeneous distribution. Therefore, a chiral CTQW which evolves to nearly localized states and could be optimal for transport will also maximize $\mathcal{D}_{QC}(t)$. To further support this claim, we can

look at the phase dependence of the functions $\mathcal{C}(t)$ and $\mathcal{I}(t)$, as in Fig. 4 for a 5-cycle. Again, the resonant phase (black line, $\theta = \frac{\pi}{10}$) is associated with higher localization (lower coherence and higher IPR values) especially at short times, and also the overall trend seen for the quantum-classical distance is respected at least at short times, with values of θ close to zero leading to the opposite behavior. We conclude this section by noting that some results about so-called *pretty good universal transport* for chiral CTQW on cycles with a prime number of vertices are known in the mathematical literature [29], although they have little role in a physical context since no bound on the time needed for transport is considered there.

V. COMPLETE GRAPHS

Having discussed cycle graphs characterized by minimal connectivity, we will now examine the regular graphs with maximal connectivity, i.e., complete graphs. In a complete graph just a minority of phases of H can be ignored by gauge
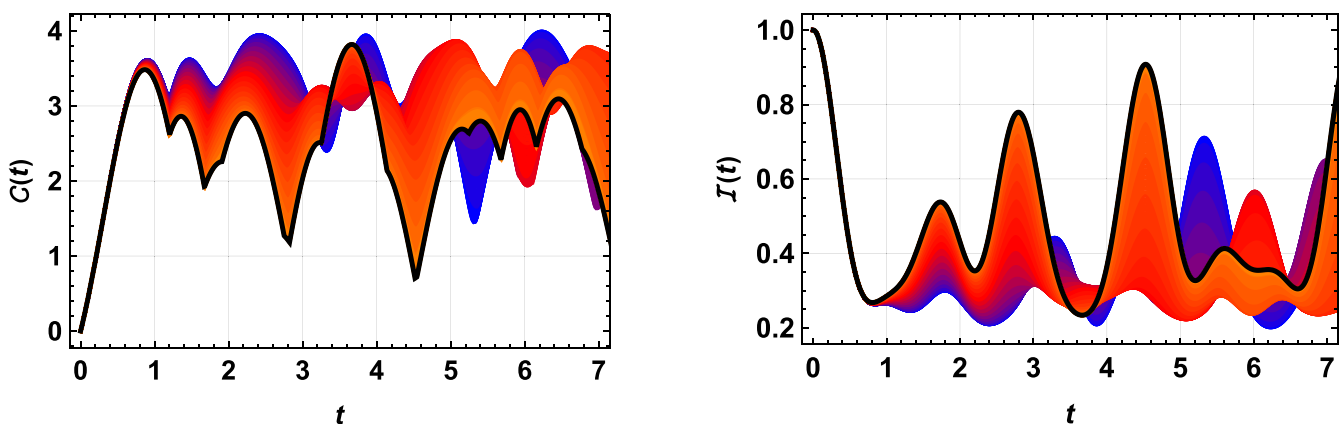

FIG. 4. Coherence and IPR vs time for a 5-cycle and for different values of $\theta \in [0, \frac{\pi}{10})$, corresponding to color shades from blue to orange (from darker to lighter shade). The black (solid) line represents the resonant phase $\frac{\pi}{10}$.
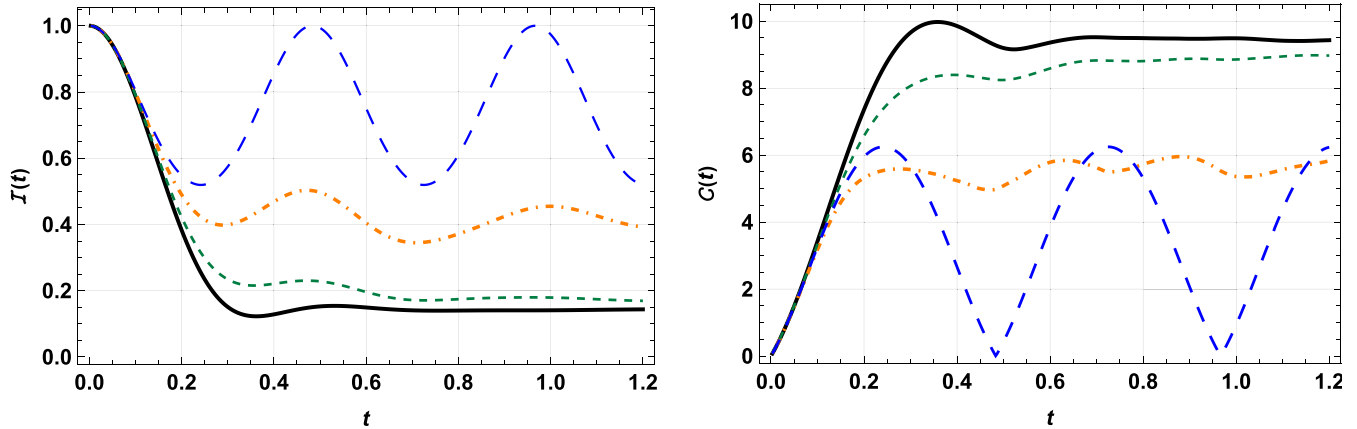
FIG. 5. IPR $\mathcal{I}(t)$ and coherence $\mathcal{C}(t)$ vs time of a continuous-time quantum walker on a complete graph with $N = 13$ sites with localized initial condition. The standard evolution generated by $H = L$ is depicted by the blue curves (space-dashed). The orange curves (dot-dashed) are averages over 400 Hamiltonians with a single, randomly generated phase attached to all links in the "positive" direction. The dark-green curves (dashed) resulted from the average of 400 Hamiltonians with two, independent, randomly generated phases randomly attributed to each link in the positive direction. Black curves (solid) correspond to the random assignment of independent phases to each link, still averaged over 400 runs.

invariance, and we expect that the role played by the new degrees of freedom will be major for this topology.

At this point it is worth mentioning that, for standard quantum walks with real Hamiltonian generators, the dynamics of the walker on a complete graph with localized starting condition is equivalent to the dynamics on a star graph with the same number of vertices, when starting at the core vertex [30]. In other words, if the Hamiltonian is real, many links of the complete graph can be eliminated without changing the evolution. This is intuitive by symmetry arguments: since all vertices are connected to the initial one, the amplitudes in all the vertices except the first will be equal at all times and probability will never flow through links that connect these vertices, therefore they are irrelevant for the dynamics. Interestingly, the addition of phases radically changes this conclusion since, as we shall see, search for the quantum speed limit and without an oracle can be achieved on a complete graph with appropriately chosen phases, while this is clearly impossible with the star graph which has no nontrivial phase degrees of freedom, being a tree graph. The upshot is that the generalization to Hermitian Hamiltonians and chiral CTQWs is more powerful than previously imagined because it explicitly differentiates between graph topologies that, for some initial conditions, would be completely equivalent for evolutions generated by the simple Laplacians.

A. Random chiral Hamiltonians for complete graphs

We initially investigated the effect of randomly added phases on quantum-classical distance, 1-norm of coherence and IPR. Because of the large number of free parameters, we adopted different strategies to better explore the parameters space. Figure 5 compares the averaged coherence with the IPR for different phase choices on the complete graph with $N = 13$. The blue curves corresponds to the nonchiral choice with $H = L$. The orange curves are averages over 400 configurations where a single phase $e^{i\phi}$ is generated randomly and then attached to all the links of the complete graph in

the direction $j \to k$ for $k > j$. We infer that a typical phase different from $\phi = 0$ attached to each link increases the average coherence and decreases the IPR with respect to $H = L$. If, instead, we stochastically distribute two random phases $e^{i\phi_1}$, $e^{i\phi_2}$ among the edges in the given direction, there is an even greater increase in the coherence and decrease in the IPR (dark green curves, again resulting from an average of 400 random configurations). Finally, if an independent, randomly generated phase is attached to each link, the resulting average behavior is described by the black curves. Notice that the order is now irrelevant, since all orders will be explored if the phase of each link is independent and sampled in the full range $[0, 2\pi)$. Clearly this rule entails all the previous ones, but the *typical* configuration contributing to the black curve will be one in which there is no correlation between phases on different links and there is essentially full *disorder* in the phase degrees of freedom of the Hamiltonian. Now the IPR stabilizes to the lowest values between the examined ones, while the coherence is maximal with respect to the previous cases. These two quantities therefore hint at a *phase-disorder-induced delocalization* in the evolution of a localized state on a complete graph.[4] These results were checked also for $N = 16$ and $N = 17$ and appear robust irrespective of the number of sites.

Let us now look at the difference $\Delta \mathcal{D}_{QC}$ between the quantum-classical distance for these different averaged evolutions and the quantum-classical distance for the reference case $H = L$ (Fig. 6, same color code). We see a glaring relation between this quantity and IPR or coherence: any addition of nonzero phase seems to add to the quantum-classical distance (at least *on average*), and the increase goes along with the higher delocalization, as signaled by large values of

---

[4]Here, by *phase disorder*, we mean the randomness in the choice of phases for each link, much like the disorder in the on-site potential in Anderson localization and *not* the disorder induced by uncertainty in the values of the Hamiltonian's parameters.
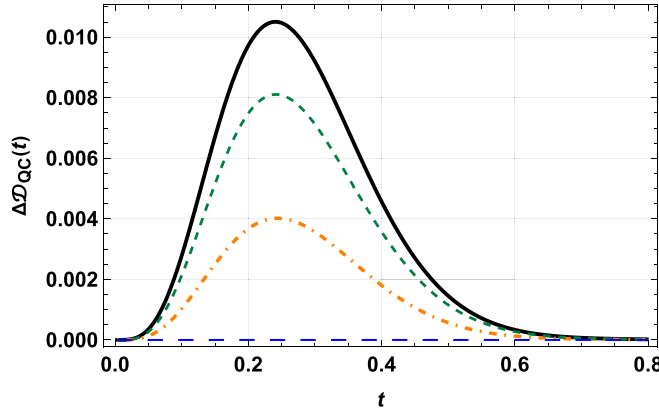
FIG. 6. Difference $\Delta\mathcal{D}_{QC}(t)$ between the quantum-classical distances of the various, averaged chiral evolutions and the nonchiral $H = L$ one, for a complete graph with $N = 13$ sites and localized initial condition of the CTQW. Color code and meaning as for Fig. 5. The reference case with $H = L$ is the base line in blue.

the coherence and low values of the IPR. Mind that, strictly speaking, we are considering the quantum-classical distance *at fixed initial state* $|j\rangle$, since the full $\mathcal{D}_{QC}(t)$ would require maximization over all initial states at each time, once H and its phases have been specified. A crucial point here is the correlation between $\Delta\mathcal{D}_{QC}$ and localization (high values of $\mathcal{I}$ and low values of $\mathcal{C}$), which is opposite with respect to the relation found for cycle graphs. Here those dynamics leading to less localized states are more quantum, according to the quantum-classical distance. This fact could be partially predicted from the short-time expansion of Eq. (17) which is not monotonic in the connectivity d_j, unlike the expansions for $\mathcal{C}(t)$ and $\mathcal{I}(t)$ to the same order in t. This is more evidence that $\mathcal{D}_{QC}(t)$ stands out against other dynamical quantities in the successful recognition of optimal chiral quantum evolutions. Of course, the relevant task is graph-dependent, being either a hitting-type or a mixing-type task, but remarkably the quantum-classical distance seems able to optimize the parameters in both scenarios.

B. Optimization of quantum-classical distance

Guided by these observations, the next natural step is to maximize $\mathcal{D}_{QC}(t)$ over all possible phase degrees of freedom in H for the complete graph. This has to be performed at a fixed time, which we chose afterwards by identifying the time at which $\mathcal{D}_{QC}$ attains its maximum; however, it seems that the increasing order of $\mathcal{D}_{QC}$ curves is time independent for complete graphs (as suggested by Fig. 6) and the result is the same if another time is set for the numerical maximization. Starting with random guesses, the optimization converges to different Hamiltonians each time. However, a common feature of these optimal matrices is easy to spot:

(1) The first column of an optimal H_O on the complete graph of N sites is orthogonal, with respect to the Hermitian product on $\mathbb{C}^N$, to all the rows of H except the first one (assuming that all the diagonal elements have been fixed to zero, without loss of generality).

The first column is singled out because of the choice of $|1\rangle$ as the (arbitrary) initial condition. Let us call $\underline{h}$ the first column of an optimal Hamiltonian H_O. Because of the topology and the choice of diagonal elements, its entries will be

$$h_1 = 0, \quad h_j = e^{i\phi_j} \ \forall \ j = 2, \dots, N, \tag{31}$$

and, since H_O is Hermitian, its first row will be $(\underline{h}^*)^T$, so that the scalar product between the first row and the first column is $N - 1$. Let us denote by $\underline{e}_1$ the localized state $|1\rangle$ in matrix notation, which is the first vector of the canonical basis. Then we have

$$\begin{aligned} H_O^{2n}\underline{e}_1 &= (N-1)^n \underline{e}_1, \\ H_O^{2n+1}\underline{e}_1 &= (N-1)^n H_O\underline{e}_1 = (N-1)^n\underline{h}. \end{aligned} \tag{32}$$

The evolution of the initial state localized at site 1 then follows immediately:

$$e^{-itH_O}\underline{e}_1 = \cos\left(\sqrt{N-1}t\right)\underline{e}_1 - \frac{i}{\sqrt{N-1}}\sin\left(\sqrt{N-1}t\right)\underline{h}. \tag{33}$$

Notice that $\underline{h}$, as a vector of amplitudes, represents a state which is balanced between all sites except the first, to which it is orthogonal. Therefore, the evolution of Eq. (33) is a cyclic rotation between the initial state localized at site 1 and the equally spread state over all other sites except the initial one, necessarily passing through an intermediate flat state:

$$|f\rangle = \frac{1}{\sqrt{N}}\left(|1\rangle + \sum_{j=2}^{N} e^{i\phi_j}|j\rangle\right), \tag{34}$$

where the amplitude to find the walker in any site of the graph is equal to $N^{-1/2}$. The time needed to reach $|f\rangle$ for the first time is given by

$$t_f = \frac{1}{\sqrt{N-1}}\arccos\frac{1}{\sqrt{N}}, \tag{35}$$

while the time needed to reach the state $|h\rangle = \frac{1}{\sqrt{N-1}}\sum_{j=2}^{N} h_j|j\rangle$ associated with the vector $\underline{h}$ and orthogonal to the initial state $|1\rangle$ is

$$t_h = \frac{\pi}{2\sqrt{N-1}}. \tag{36}$$

It should be emphasized that $|f\rangle$, as for any flat state, has maximal coherence value of $N - 1$ and minimal IPR value of $\frac{1}{N}$. Exploiting the simple structure of these optimal evolutions, an exact expression for their quantum-classical distance can also be derived:

$$\mathcal{D}_{QC}^O(t) = 1 - \frac{1 - e^{-Nt}}{N} - e^{-Nt}\frac{1 + \cos\left(2\sqrt{N-1}t\right)}{2}. \tag{37}$$

C. Search for the quantum speed limit without an oracle

Another interesting property of the "optimal" evolution described by Eq. (33) can be appreciated if we choose $|\underline{h}\rangle = \frac{i}{\sqrt{N-1}}\sum_{j=1}^{N}|j\rangle$, i.e., all the phases of the first column of H_O equal to i. This can always be achieved by an appropriate gauge transformation on any Hamiltonian that already fulfills Condition 1. In this case, $|f\rangle = \frac{1}{\sqrt{N}}\sum_{j=1}^{N}|j\rangle$ is the flat state

with relative phases all equal, therefore the backwards evolution from $|f\rangle$ is a *solution to the search problem* with target vertex 1, starting from the unbiased state and without an oracle (but with biased phases), in a time t_f, i.e., $e^{iH_0 t_f}|f\rangle = |1\rangle$.

Since coherence and IPR for a localized initial condition are gauge-invariant quantities, the blue curves in Fig. 5 imply that it is not possible to reach a flat state from a localized state with any H which is gauge-equivalent to L. Thus, Condition 1 and our result for the search problem *require a nontrivial configuration* of the phase degrees of freedom. It is interesting to compare our search time t_f with Grover's time and with the quantum speed limit for this evolution. Grover's time t_g is the time required for the Grover's Hamiltonian $H_G = L - N|1\rangle\langle 1|$ to search for the state $|1\rangle$ when starting from the flat state $|f\rangle$. The operator $N|1\rangle\langle 1|$, called the *oracle*, is needed to break the symmetry between all the vertices of the complete graph and to guide the evolution towards the target vertex. For a complete graph with N vertices, Grover's time is

$$t_g = \frac{\pi}{2\sqrt{N}}. \tag{38}$$

For any $N > 2$ one has $t_f < t_g < t_h$, therefore our search Hamiltonian is *faster* than Grover's one, and does not require an oracle. Of course, in order for this result to hold, a bias has to be present in the *phases* of our optimal H so that the target vertex can be singled out during the evolution. This bias is in fact embodied by Condition 1. In particular, one can contrast this result with the one in Ref. [31], where the oracle was preserved but only unbiased choices of phases were considered, concluding that no improvement of search time was possible. It is now meaningful to ask whether this time t_f reaches the ultimate time bound allowed by quantum mechanics for the evolution between these initial and final states. To this end, we briefly recall the notion of quantum speed limits [32–35]. Consider two states $|a\rangle$, $|b\rangle$ on a Hilbert space $\mathcal{H} \sim \mathbb{C}^N$ that have the *same* average energy[5] with respect to a time-independent Hamiltonian operator $\hat{H}$ on $\mathcal{H}$. Then the *quantum speed limit* τ_{QSL} is a lower bound on the time needed for the unitary evolution $e^{-it\hat{H}}$ to rotate $|a\rangle$ to $|b\rangle$, and it is provided by the following expression:

$$\tau_{\mathrm{QSL}} := \max \left\{ \frac{\arccos |\langle b|a\rangle|}{\Delta \hat{H}} , \frac{2(\arccos |\langle b|a\rangle|)^2}{\pi (\langle \hat{H}\rangle - E_0)} \right\}, \tag{39}$$

where $\Delta \hat{H} = (\langle \hat{H}^2\rangle - \langle \hat{H}\rangle^2)^{1/2}$ is the standard deviation of energy of the states($|a\rangle$ or $|b\rangle$), $\langle \hat{H}\rangle$ is their average energy, and E_0 is the ground-state energy. The first quantity inside the max of the quantum speed limit can be readily computed in our case, for $|a\rangle = |f\rangle$ and $|b\rangle = |1\rangle$; indeed, the variance $\Delta \hat{H}$ does not depend on the phases and it is equal to $\sqrt{N-1}$ for any Hamiltonian with constant diagonal terms and compatible with the complete graph's topology. Therefore,

$$\frac{\arccos |\langle 1|f\rangle|}{\Delta \hat{H}} = \frac{1}{\sqrt{N-1}} \arccos \frac{1}{\sqrt{N}} = t_f. \tag{40}$$

Since we already know that t_f cannot be smaller than τ_{QSL}, the max in the definition (39) of τ_{QSL} and the result of Eq. (40)
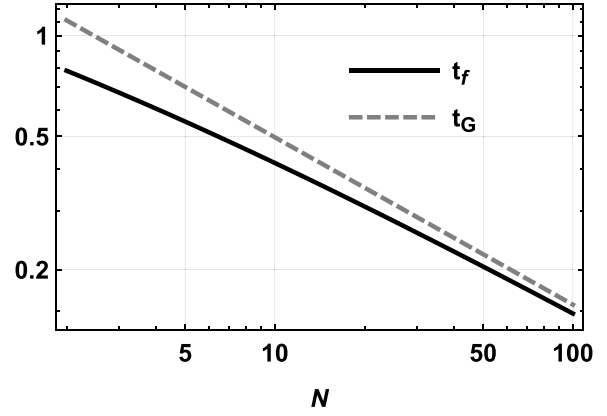

FIG. 7. Optimal search time exploiting phases t_f (black line) and Grover's time t_G as functions of the number of sites N, with log scale on both axes. t_f is always smaller than t_G, and it is also equal to the quantum speed limit τ_{QSL}.

already imply that $\tau_{\mathrm{QSL}} = t_f$. This was verified by computing the second quantity in Eq. (39) and checking that it is always smaller than the first for $N > 3$.[6] It can be shown that τ_{QSL} is also the quantum speed limit for Grover's Hamiltonian. Indeed, we highlight that $\Delta \hat{H}$ attains its largest value for the complete graph, among all the topologies that connect N vertices in a simple, connected graph. We conclude that our construction exploits phases to achieve a quantum search between N orthogonal states without an oracle and in the least possible time allowed by quantum mechanics, without altering the on-site energies at will. We remark that the scaling behavior $O(N^{-1/2})$ of Grover's time is known to be already the best one, and indeed our search time t_f follows the same asymptotic scaling for large N. The construction that we provided, on the other hand, achieves the goal of optimizing the constant prefactor, which is suboptimal for Grover's algorithm. The comparison in log-scale is shown in Fig. 7.

To further illustrate the differences between the evolution induced by Grover's Hamiltonian H_G and the optimal solution H_O that we found, we plotted in Fig. 8 the time behavior of the quantities $\mathcal{C}(t)$, $\mathcal{I}(t)$ and also the gain in quantum-classical distance $\Delta \mathcal{D}_{QC}$ with respect to the reference $H = L$, again for a complete graph with $N = 13$ sites and starting at vertex $|1\rangle$. Black curves depict the evolution generated by H_O, while Grover's evolution is in light-green. The blue curves correspond to the nonchiral $H = L$ choice. The insets show a magnification of the regions where the relevant times happen: the red circle indicates the time t_f, the red square designates time t_G and finally the rotated square indicates t_h.

Importantly, the gain in quantum-classical distance with respect to the nonchiral $H = L$ choice is also maximal for the evolution generated by H_O, even when compared with Grover's evolution, a nonobvious fact since the maximization was performed without considering diagonal degrees of freedom. Moreover, the optimal evolution outperforms the best

---

[5]This is clearly a necessary condition in order for the unitary evolution generated by $\hat{H}$ to bring $|a\rangle$ to $|b\rangle$.

[6]The check was performed numerically because E_0 depends on the phases in a nontrivial way, so that the second quantity is harder to compute in general.
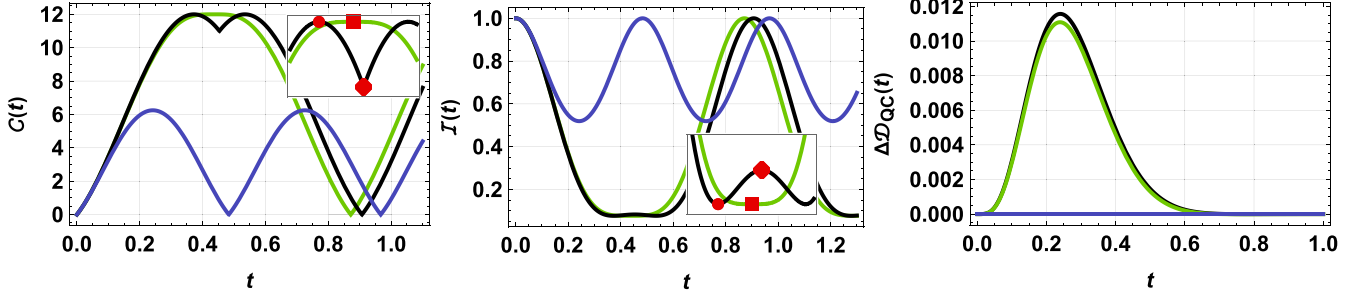
FIG. 8. Comparison for coherence $\mathcal{C}(t)$, IPR $\mathcal{I}(t)$, and gain $\Delta\mathcal{D}_{QC}(t)$ in quantum-classical distance for evolutions generated by H_O (black curves), H_G (light-green curves), and $H = L$ (blue curves) for a complete graph of $N = 13$ sites and starting with a localized state. The insets in plots of $\mathcal{C}(t)$ and $\mathcal{I}(t)$ show a magnification of the region for $0.3 < t < 0.5$, where times t_f (red circle), t_G (red square), and t_h (rotated red square) are located.

evolutions found in Fig. 5 by randomly generating phases according to IPR and coherence, and correspondingly $\Delta\mathcal{D}_{QC}$ is, in fact, higher at all times.

It remains to be shown that Condition 1 can indeed be fulfilled by some choice of phases for any N without relying on the optimization of $\mathcal{D}_{QC}$. This is carried out in detail in Appendix, but it should be clear that Condition 1 arose solely from the maximization of the quantum-classical distance, thereby corroborating the power of this method.

To conclude with this class of examples, let us remark that, with nonchiral CTQWs on complete graphs with N vertices, it is impossible to observe *instantaneous uniform mixing* [26], where the walker completely delocalizes to a uniform superposition of all basis states at a certain instant during its evolution, except for $N = 2, 3, 4$. Our result shows that, with the generalization to *chiral* quantum walks, but retaining unitarity, instantaneous uniform mixing is achievable on *any* complete graph in a remarkably short time t_f given by Eq. (35), which is $O(1/\sqrt{N})$ for large N. Importantly, this is a quadratic speedup with respect to the $O(1)$ scaling of mixing on hypercube graphs [25][7] and it also holds for generic number of sites, whereas the hypercube protocol applies only if N is a power of 2.

VI. QUANTUM SWITCHES

Here we consider graphs like the one depicted in Fig. 9, which are seldom referred to as *quantum switches*. Since the graph is planar and there is a single loop, just one phase will affect transition probabilities between sites, and we attach it on the link which closes the triangle and is opposite to vertex 1, calling it $e^{i\phi}$ in the direction specified in the figure.

These graphs were considered in Ref. [21] as examples of the advantage provided by *chiral* quantum walks over those defined by the Laplacian or the adjacency matrix. Indeed, it was shown that a resonant value of $\phi = \frac{\pi}{2}$ suppresses trans-

port from vertex 1 to vertex 11, with reference to Fig. 9, while enhancing transport from vertex 1 to vertex 12. Unlike all the other graphs considered so far, the quantum switch is nonregular, meaning that the connectivity is not the same for all sites and the Laplacian or the adjacency matrix of the graph generates different quantum evolutions. Here we first consider the adjacency matrix A for a 12-site switch, and then attach a phase to the link between vertex 5 and vertex 6. In Fig. 10 we again plot the difference between $\mathcal{D}_{QC}(t)$ for the Hamiltonian with such a phase and the same quantity without the phase. The value of ϕ is increasing between 0 and $\frac{\pi}{2}$ from light gray to black curves, and we checked that larger values of ϕ are redundant.

The comparison with coherence and IPR shows a similar relation to that seen for cycle graphs: more localized evolutions, leading to higher values of IPR and lower values of coherence, are associated with higher gains in $\Delta\mathcal{D}_{QC}$. The resonant phase $\phi = \frac{\pi}{2}$ is clearly identified as the black curve which maximizes $\Delta\mathcal{D}_{QC}$. It achieves a transport fidelity of ≈ 0.77 to the target state $|12\rangle$ when starting in $|1\rangle$ in a time $t \approx 5$. Surprisingly, this transport probability is considerably higher than the value that would be reached in a comparable time range for a simple chain of eight sites, i.e., if the third arm of the triangle (composed of vertices 6, 7, 9, and 11) were

---

[7]In the literature on quantum algorithms, it is common wisdom to rescale the adjacency matrix of regular graphs by their connectivity to compare evolution times. With that convention, the time needed to achieve uniform mixing with the scaled adjacency matrix on hypercube graphs is $O(N)$, while the time to perform the same task on complete graphs with our *chiral* protocol is $O(\sqrt{N})$.
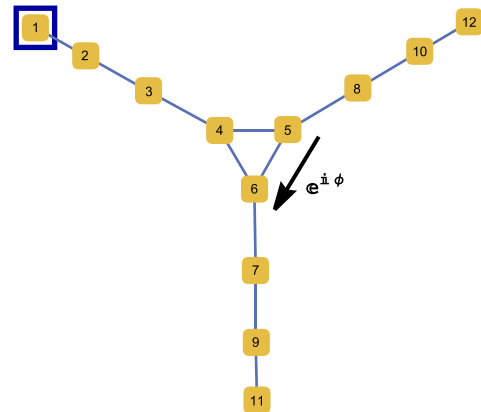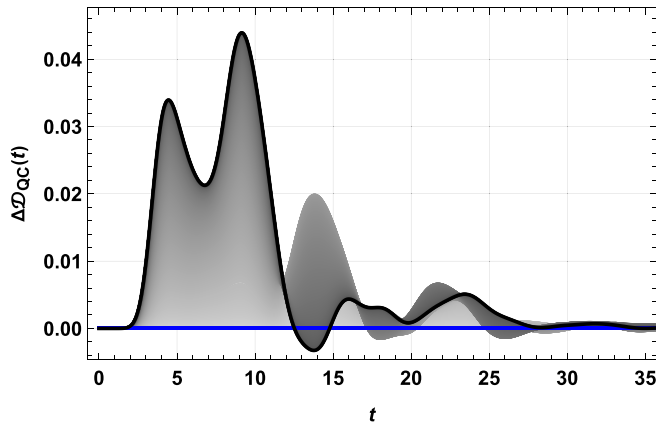

FIG. 9. Graph of the quantum switch with 12 sites. The walker starts at site 1 (boxed in blue) and the link between site 5 and site 6 bears a phase of $e^{i\phi}$ in the Hamiltonian (black arrow).

FIG. 10. Difference between $\mathcal{D}_{QC}$ for the adjacency matrix of the 12-site quantum switch with an adjoined phase and the same quantity for the standard adjacency matrix. The value of ϕ ranges from 0 to $\frac{\pi}{2}$ for increasingly darker shades of gray. The black line results from the resonant phase $\frac{\pi}{2}$ and the blue baseline (horizontal) is the nonchiral evolution.

not there to begin with, assuming the Laplacian as generator in this latter case.

When we take the Laplacian in place of the adjacency matrix as the starting point, instead, the result differs qualitatively. Now for any choice of the free phase, localization on one branch of the switch is never as effective as the previous case. Accordingly, $\mathcal{D}_{QC}$ attains lower values now and its variations with phases are smaller, favoring the choice $H = A$ for quantum transport on this topology. This example also provides further motivation in favor of the use of the adjacency matrix in place of the Laplacian for CTQWs on finite, nonregular graphs. Indeed, while having the connectivities on the diagonal is natural if the differential form of the Laplacian has to be recovered in the continuum limit (without an additional potential field landscape), this request is not so meaningful for small, nonregular graphs that do not embody a discretization of a continuous space in any obvious way.

VII. CUBE GRAPH

On the cube graph, perfect transport between opposite vertices is possible with a standard CTQW [12]. Moreover, being part of the hypercubes family, the CTQW starting from any localized state will evolve unitarily towards a maximally coherent state, exhibiting instantaneous uniform mixing [25]. In other words, both goals considered in this work are already achieved by a standard, nonchiral CTQW on the cube graph. Notice also that, once the phase degrees of freedom are taken into account, instantaneous uniform mixing and search without an oracle become equivalent: if the former is possible, starting from a localized state, the final uniform state will in general encode the information about the starting vertex in the relative phases. These can be transferred to the Hamiltonian with a gauge transformation, then by reversing the sign of H one obtains a chiral CTQW which evolves the uniform state with no relative phases toward a localized one, effectively performing a search without an oracle. However, since this is achieved just by a gauge transformation, it will not affect $\mathcal{D}_{QC}$

and it is for all purposes equivalent to the initial nonchiral CTQW. In accordance with these observations, the optimization of the quantum-classical distance over the phase degrees of freedom on the cube graph does not provide better options: the best case for quantum hitting and mixing is already the nonchiral one. On the other hand, by minimizing $\mathcal{D}_{QC}(t)$ at short times, one finds a choice of phases that completely suppresses transport to half of the vertices of the cube, more precisely to those that are not connected to the starting one.

VIII. CONCLUSION

The opportunities stemming from a generalization of the dynamical generator of continuous-time quantum walks to a generic Hermitian matrix compatible with the graph topology have just begun to be explored and recognized in the quantum information literature. Together with the new phase degrees of freedom that permit this generalization, also comes the issue of finding the best Hamiltonian for a certain quantum task on a given graph topology. After defining continuous-time classical and (chiral) quantum walks on graphs and gauge transformations on the latter, we put at the center three gauge-invariant dynamical quantities that should help the exploration of the effects of the phase degrees of freedom on the evolution of chiral CTQW. The first two, namely the 1-norm of coherence in the on-site basis and the inverse participation ratio, quantify the degree of quantum coherence and of localization of quantum walker's state at any given time, the former being relevant because it is an inherently quantum property, while the latter can spot quantum transport. The third dynamical indicator is the quantum-classical distance, which aims at gauging the difference between a (possibly chiral) quantum evolution and the unique classical one on the same graph. Comparing the short-time expansions of the three indicators, we see that there is a correlation between them, but with no unambiguous common structure. Relying on four significant examples of graphs (some of which are actually infinite graph families) we argue that the quantum-classical distance effectively spots the "optimal" chiral quantum walk from the point of view of different tasks, depending on the topology.

Cycle graphs provide the first example and a test bed for the proposal, since some analytical results can be derived in this simple case. The maximization of $\mathcal{D}_{QC}(t)$ with respect to the phase correctly suggests that quantum transport on odd cycles is enhanced for a resonant value of the phase, while confirming that on even cycles the standard choice of the Laplacian is already the best one. For complete graphs, the number of relevant phases is very large, and a preliminary exploration of the parameters space by randomly generating chiral Hamiltonians suggests a clear correlation between greater values of $\mathcal{D}_{QC}$ and *phase-disorder-induced delocalization*, witnessed by low values of IPR and high values of coherence when all phases are random and independent. A systematic maximization of $\mathcal{D}_{QC}(t)$ (at short, fixed times) indeed identifies a chiral quantum evolution on the complete graph which achieves maximal coherence and lowest IPR in very short times. A neat property of these optimal Hamiltonians is recognized, allowing us to show that they can be used for quantum search for the optimal quantum speed limit and without an oracle, outperforming Grover's algorithm in the constant prefactor.

The third example is already known from the literature on chiral CTQWs as a *quantum switch*. Again, maximization of $\mathcal{D}_{QC}(t)$ identifies the best phase for directional transport on these topologies. Also, since these graphs are not regular, an ambiguity between the use of the Laplacian or of the adjacency matrix arises, and we argue that the latter is better for directional transport and perhaps more natural.

Finally, we examined the cube graph, which is known to exhibit perfect quantum transport for $H = L$, as part of the family of hypercubes. Numerical simulations suggest that indeed, for this topology, the standard nonchiral case has already the highest value of $\mathcal{D}_{QC}(t)$ against all other possible choices of phases, indicating that faster quantum transport could be impossible here (without *ad hoc* modifications of on-site energies). However, the *minimal* value of the quantum-classical distance also spots an interesting chiral dynamics, where half of the vertices of the cube, namely, those disjoint from the initial one, are never visited by the walker. Together with analogous conclusions for even cycles, this suggests that *minimization* of $\mathcal{D}_{QC}(t)$ can identify *suppression of transport* whenever this can happen.

In conclusion, it is worth emphasizing that an easy, general way to design new quantum algorithms with quantum walks is still missing, also because the characterization of the tasks that can be achieved efficiently on each topology is incomplete. In this light, the fact that a single quantity such as the $\mathcal{D}_{QC}(t)$ can reliably identify peculiar quantum evolutions even in the presence of a large parameters space is quite remarkable, and the *a posteriori* selection of the task should not be seen as a drawback, but rather as an opportunity to discover new phenomena, as we clearly showed with the example of search for the quantum speed limit on the complete graph. More generally, in this work we argued that if certain phases configurations do not affect much the value of $\mathcal{D}_{QC}$ then the corresponding chiral QW cannot have a significantly greater advantage with respect to the nonchiral QW, whereas another phases configuration which attains larger values of the quantum-classical distance will exhibit a more peculiar departure from the classical evolution and, therefore, possibly a stronger quantum advantage. In the future, we foresee the possibility that the quantum-classical distance could be adopted also as a cost function in a machine learning approach to design new quantum algorithms based on CTQWs.

APPENDIX: EXPLICIT CONSTRUCTION OF COMPLETE GRAPH CHIRAL HAMILTONIANS FOR QUANTUM SEARCH FOR THE SPEED LIMIT

First notice that, for any $N \geqslant 4$, Condition 1 cannot be fulfilled by simply filling the off-diagonal entries of H with any combination of ± 1 and zeros on the diagonal (with the constraint of having a Hermitian matrix compatible with the complete graph's topology). One has necessarily to resort to complex numbers. When N is even, a combination of $\pm i$ does the trick. Indeed, by choosing

$$[H]_{1j} = i, \quad [H]_{jj} = [H]_{11} = 0 \ \forall \ j = 2, \ldots, N,$$
$$[H]_{jk} = (-1)^{j+k} i \ \forall \ k > j > 1,$$

(A1)

and with the Hermitian constraint $[H]_{jk} = [H]_{kj}^* \ \forall \ j, k = 1, \ldots, N$. It is immediate to check that indeed, for N even, the first column of H is orthogonal to all the rows except the first one, with which it has an inner product of $N - 1$. For example, for $N = 6$,

$$H = \begin{pmatrix} 0 & i & i & i & i & i \\ -i & 0 & -i & i & -i & i \\ -i & i & 0 & -i & i & -i \\ -i & -i & i & 0 & -i & i \\ -i & i & -i & i & 0 & -i \\ -i & -i & i & -i & i & 0 \end{pmatrix}. \quad (A2)$$

For odd N, we found the following construction:

$$[H]_{1j} = -i, \quad [H]_{jj} = [H]_{11} = 0 \ \forall \ j = 2, \ldots, N,$$
$$[H]_{jk} = \exp\left\{ \frac{2\pi i}{N-2} \left[k - j + \frac{N-3}{2} \right] \right\} \ \forall \ k > j > 1.$$

(A3)

For example, for $N = 5$,

$$H = \begin{pmatrix} 0 & i & i & i & i \\ -i & 0 & e^{-\frac{2i\pi}{3}} & 1 & e^{\frac{2i\pi}{3}} \\ -i & e^{\frac{2i\pi}{3}} & 0 & e^{-2i\frac{\pi}{3}} & 1 \\ -i & 1 & e^{\frac{2i\pi}{3}} & 0 & e^{-\frac{2i\pi}{3}} \\ -i & e^{-\frac{2i\pi}{3}} & 1 & e^{\frac{2i\pi}{3}} & 0 \end{pmatrix}. \quad (A4)$$

[1] V. M. Kendon and C. Tamon, Perfect state transfer in quantum walks on graphs, J. Comp. Theor. Nanosci. **8**, 422 (2011).

[2] O. Mülken and A. Blumen, Continuous-time quantum walks: Models for coherent transport on complex networks, Phys. Rep. **502**, 37 (2011).

[3] L. Razzoli, M. G. A. Paris, and P. Bordone, Transport efficiency of continuous-time quantum walks on graphs, Entropy **23**, 85 (2021).

[4] N. Kulvelis, M. Dolgushev, and O. Mülken, Universality at Breakdown of Quantum Transport on Complex Networks, Phys. Rev. Lett. **115**, 120602 (2015).

[5] D. Tamascelli, S. Olivares, S. Rossotti, R. Osellame, and M. G. A. Paris, Quantum state transfer via Bloch oscillations, Sci. Rep. **6**, 26054 (2016).

[6] D. Ferracin, A. Mattioni, S. Olivares, F. Caycedo-Soler, and D. Tamascelli, Which-way interference within ringlike unit cells for efficient energy transfer, Phys. Rev. A **99**, 062505 (2019).

[7] F. Zatelli, C. Benedetti, and M. G. A. Paris, Scattering as a quantum metrology problem: A quantum walk approach, Entropy **22**, 1321 (2020).

[8] J. Kempe, Quantum random walks: An introductory overview, Contemp. Phys. **44**, 307 (2003).

[9] M. Mohseni, P. Rebentrost, S. Lloyd, and A. Aspuru-Guzik, Environment-assisted quantum walks in photosynthetic energy transfer, J. Chem. Phys. **129**, 174106 (2008).

[10] A. W. Chin, A. Datta, F. Caruso, S. F. Huelga, and M. B. Plenio, Noise-assisted energy transfer in quantum networks and light-harvesting complexes, New J. Phys. **12**, 065002 (2010).

[11] A. M. Childs, Universal Computation by Quantum Walk, Phys. Rev. Lett. **102**, 180501 (2009).

[12] A. M. Childs and J. Goldstone, Spatial search by quantum walk, Phys. Rev. A **70**, 022314 (2004).

[13] R. Portugal, *Quantum Walks and Search Algorithms* (Springer Nature Switzerland, AG, 2018).

[14] A. M. Childs and Y. Ge, Spatial search by continuous-time quantum walks on crystal lattices, Phys. Rev. A **89**, 052337 (2014).

[15] S. Chakraborty, L. Novo, A. Ambainis, and Y. Omar, Spatial Search by Quantum Walk is Optimal for Almost All Graphs, Phys. Rev. Lett. **116**, 100501 (2016).

[16] S. Chakraborty, L. Novo, and J. Roland, Optimality of spatial search via continuous-time quantum walks, Phys. Rev. A **102**, 032214 (2020).

[17] M. G. A. Paris, C. Benedetti, and S. Olivares, Improving quantum search on simple graphs by pretty good structured oracles, Symmetry **13**, 96 (2021).

[18] M. Roget, S. Guillet, P. Arrighi, and G. Di Molfetta, Grover Search as a Naturally Occurring Phenomenon, Phys. Rev. Lett. **124**, 180501 (2020).

[19] E. Farhi and S. Gutmann, Quantum computation and decision trees, Phys. Rev. A **58**, 915 (1998).

[20] A. M. Childs, E. Farhi, and S. Gutmann, An example of the difference between quantum and classical random walks, Quantum Inf. Process. **1**, 35 (2002).

[21] Z. Zimborás, M. Faccin, Z. Kádá, J. D. Whitfield, B. P. Lanyon, and J. Biamonte, Sci. Rep. **3**, 2361 (2013).

[22] D. Lu, J. D. Biamonte, J. Li, H. Li, T. H. Johnson, V. Bergholm, M. Faccin, Z. Zimborás, R. Laflamme, J. Baugh, and S. Lloyd, Chiral quantum walks, Phys. Rev. A **93**, 042302 (2016).

[23] M. Frigerio, C. Benedetti, S. Olivares, and M. G. A. Paris, Generalized quantum-classical correspondence for random walks on graphs, Phys. Rev. A **104**, L030201 (2021).

[24] V. Gualtieri, C. Benedetti, and M. G. A. Paris, Phys. Rev. A **102**, 012201 (2020).

[25] C. Moore and A. Russell, Quantum Walks on the Hypercube, *Proceedings of the 6th Int. Workshop on Randomization and Approximation in Computer Science (RANDOM'02)*; arXiv:quant-ph/0104137.

[26] A. Ahmadi, R. Belk, C. Tamon, and C. Wendler, On mixing in continuous-time quantum walks on some circulant graphs, Quantum Inf. Comput. **3**, 611 (2003).

[27] T. G. Wong, L. Tarrataca, and N. Nahimov, Laplacian versus adjacency matrix in quantum walk search, Quantum Inf. Process. **15**, 4029 (2016).

[28] J. W. Turner and J. Biamonte, Topological classification of time-asymmetry in unitary quantum processes, J. Phys. A: Math. Theor. **54**, 235301 (2021).

[29] S. Cameron, S. Fehrenbach, L. Granger, O. Hennigh, S. Shrestha, and C. Tamon, Universal state transfer on graphs, Lin. Alg. Appl. **455**, 115 (2014).

[30] X.-P. Xu, Exact analytical results for quantum walks on star graphs, J. Phys. A: Math. Theor. **42**, 115205 (2009).

[31] T. G. Wong, Quantum walk search with time-reversal symmetry breaking, J. Phys. A: Math. Theor. **48**, 405303 (2015).

[32] V. Giovannetti, S. Lloyd, and L. Maccone, Quantum limits to dynamical evolution, Phys. Rev. A **67**, 052109 (2003).

[33] V. Giovannetti, S. Lloyd, and L. Maccone, The quantum speed limit, in *Fluctuations and Noise in Photonics and Quantum Optics*, edited by D. Abbott, J. H. Shapiro, and Y. Yamamoto, *International Society for Optics and Photonics* (SPIE, 2003), Vol. 5111, pp. 1–6.

[34] V. Giovannetti, S. Lloyd, and L. Maccone, The speed limit of quantum unitary evolution, J. Opt. B: Quantum Semiclassical Opt. **6**, S807 (2004).

[35] S. Deffner and S. Campbell, Quantum speed limits: From Heisenberg's uncertainty principle to optimal quantum control, J. Phys. A: Math. Theor. **50**, 453001 (2017).